A new probe of magnetic fields in the pre-reionization epoch: II. Detectability

Vera Gluscevic,[1] Tejaswi Venumadhav,[1] Abhilash Mishra,[2] Antonija Oklopcic,[2] and Christopher Hirata[3]

[1] *Institute for Advanced Study, Einstein Drive, Princeton, NJ 08540, USA*
[2] *California Institute of Technology, Mail Code 350-17, Pasadena, CA 91125, USA*
[3] *Center for Cosmology and Astroparticle Physics, The Ohio State University, 191 West Woodruff Lane, Columbus, Ohio 43210, USA*

(Dated: November 25, 2015)

In the first paper of this series, we proposed a novel method to detect large-scale magnetic fields in the Dark Ages, using 21-cm tomography surveys. In this paper, we examine detectability of magnetic fields using this method. We first develop a minimum-variance estimator formalism to measure magnetif fields using the characteristic anisotropic imprints in the 21-cm brightness-temperature 2-point correlation functions. We then evaluate Fisher expressions for this estimator and find that a radio array presenting about a square kilometer of area covered in dipole antennas (such as the next-generation of HERA, or the SKA in a tightly-packed configuration) can detect fields of strength on the order of 10^{-21} Gauss (scaled to present day)—almost 10 orders of magnitude below the CMB constraints. Measurement of the field strength will, however, require more futuristic arrays.

I. INTRODUCTION

Magnetic fields are ubiquitous in the universe on all observed scales [1–5]. However, the origins of the magnetic fields in Galaxies and on large scales are as of yet an unresolved question. Various forms of dynamo mechanisms [6] are proposed to maintain and amplify magnetic fields, but they typically require seed fields to act [1]. The seed fields may be produced during structure formation through Biermann battery or similar mechanisms [7, 8], or otherwise may be relics from the early universe [1, 9, 10]. Observations of large-scale weak magnetic fields in the high-redshift intergalactic medium (IGM) can thus provide tools for understanding the origins of magnetic fields in the present-day universe, and potentially open up an entirely new window into the physics of the early universe.

Many observational probes have previously been used to search for evidence of large-scale magnetic fields locally and at high redshifts; see, e. g. [4, 11–19]. Amongst the most sensitive tracers of cosmological magnetic fields are the measurements of the cumulative effect of Faraday rotation in the cosmic-microwave-background polarization maps, which currently place an upper limit of $\sim 10^{-10}$ Gauss (in comoving units) using the data from the Planck sattelite [20]. In Paper I of this series [21], we proposed a novel method to detect and measure extremely weak cosmological magnetic fields during the pre-reionization epoch (the Dark Ages). This method relies on future 21-cm brightness-temperature tomography surveys [22, 23], many of which have pathfinder experiments currently running [24–29], and plans for the next stages to be realized in the coming decade [27, 29]. As we show in Paper I, the measurement of statistical anisotropy in the 21-cm signal from the Dark Ages has intrinsic sensitivity to magentic fields in the IGM more than *10 orders of magnitude below the current upper limits.*

While Paper I layed out the formalism necessary to account for the effect of magnetic fields on the statistics of the 21-cm signal, this paper (which we refer to as Paper II in the following) focuses on evaluating the sensitivity of future 21-cm experiments using this method. The rest of this paper is organized as follows. In §II, we present a quick overview of the main results in Paper I. In §IV, we derive minimum-variance estimators for a uniform and stochastic magnetic field. In §V, we set up the Fisher analysis formalism necessary to evaluate detectability. In §VI, we present numerical results, and we conclude in §VII. Supporting materials are presented in the appendicies.

II. SUMMARY OF THE METHOD

Magnetic moments of hydrogen atoms in the excited state of the 21-cm line transition tend to be aligned with the incident quadrupole of the 21-cm radiation from the surrounding medium. This effect of "ground-state alignment" [30, 31] arises in a cosmological setting due to velocity-field gradients. In the presence of external large-scale magnetic fields, the emitted 21-cm quadrupole is misaligned with the incident quadrupole, due to atomic precession (illustrated in Figure 1). The resulting emission anisotropy can thus be used to trace magnetic fields at high redshifts.

The main result of Paper I was a calculation of the 21-cm brightness temperature $T_{\rm b}$ as a function of the line of sight (LOS) direction $\widehat{\mathbf{n}}$, in the frame of the emitting ensamble of atoms. The relevant expression is

$$\begin{aligned}\delta T_{\rm b}(\widehat{\mathbf{n}}) &= \left(1-\frac{T_\gamma}{T_{\rm s}}\right) x_{1\rm s}\left(\frac{1+z}{10}\right)^{1/2} \\ \times&\Bigg[26.4\ {\rm mK}\Big\{1+\left(1+(\widehat{\mathbf{k}}\cdot\widehat{\mathbf{n}})^2\right)\delta\Big\} - 0.128\ {\rm mK}\left(\frac{T_\gamma}{T_{\rm s}}\right) \\ &\times x_{1\rm s}\left(\frac{1+z}{10}\right)^{1/2}\Big\{1+2\left(1+(\widehat{\mathbf{k}}\cdot\widehat{\mathbf{n}})^2\right)\delta \\ &-\frac{\delta}{15}\sum_m \frac{4\pi}{5}\frac{Y_{2m}(\widehat{\mathbf{k}})\left[Y_{2m}(\widehat{\mathbf{n}})\right]^*}{1+x_{\alpha,(2)}+x_{{\rm c},(2)}-imx_{\rm B}}\Big\}\Bigg],\end{aligned} \tag{1}$$

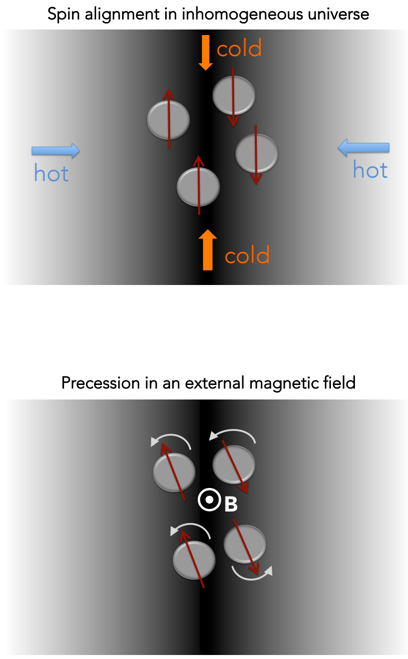

Figure 1. Illustration of the effect of a magnetic field on hydrogen atoms in the excited state of 21-cm transition at high redshifts. In the classical picture, magnetic moments of the atoms (depicted as red arrows) tend to be aligned with density gradients (upper panel; the gradient is depicted with the background shading), unless they precess about the direction of ambient magnetic field (pointing out of the page on the lower panel). When the precessing atoms decay back into the ground state, the emitted quadrupole (aligned with the direction of the magnetic moments) is misaligned with the incident quadrupole. This offset can be observed as a statistical anisotropy of 21-cm-brightness-temperature correlation functions, and used to trace cosmological magnetic fields.

where $x_{\alpha,(2)}$, $x_{c,(2)}$ and x_B parametrize the rates of depolarization of the ground state by optical pumping, collisions, and magnetic precession (relative to radiative depolarization), respectively (defined in detail in Paper I). Furthermore, T_s and T_γ are the spin temperature and the temperature of the cosmic microwave background at redshift z, respectively; $\widehat{\mathbf{k}}$ is a unit vector in the direction of the wave-vector $\vec{k}$ of a given density Fourier mode; and Y_{2m} represent the usual spin-zero spherical harmonics. Figure 2 illustrates the effect of the magnetic field on the brightness temperature emission pattern in the frame of the atom; shown are quadrupole patterns corresponding to the sum-term of Eq. (1), for various strengths of the magnetic field. Notice that there is a saturation limit for the field strength—for strong enough fields, the precession time is much smaller than the lifetime in the excited state, and when the emission pattern assymptotes to the one shown in the bottom panel of Figure 2. Above this limit, approximation of linear dependence of T_b breaks down, which implies that the signal cannot be used to reconstruct the strength of the field; however, it is still possible to distinguish saturated regime from the case of null field, as we will see in §V.

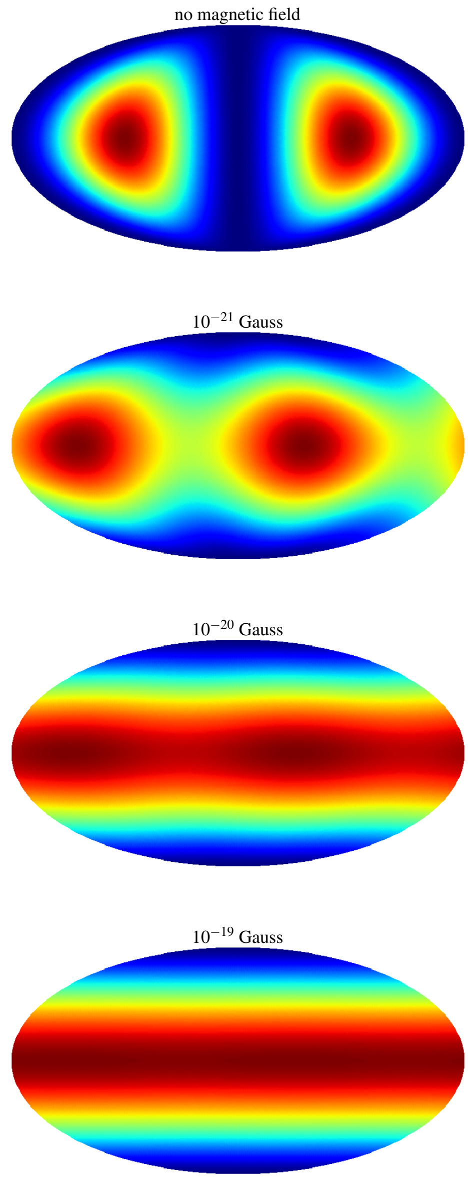

Figure 2. Illustration of the quadrupolar pattern of 21-cm emission from the last (B-dependent) term of Eq. (1) in the frame of the emitting atoms, for the case where $\vec{k}$ is perpendicular to $\widehat{\mathbf{n}}$ (maximal signal), shown in Molleweide projection. Lower panels correspond to increasingly stronger magnetic fields (strength denoted on each panel in comoving units), with the bottom panel corresponding to the saturated case. Notice how the type of quadrupole differs for the no-magnetic field case and the case the field is "strong" in the saturation sense.

The affect of quadrupole misalignement arises at second order in optical depth (it is a result of a two-scattering process), and is thus a small correction to the total brightness temperature. However, owing to the long lifetime of the excited state (during which even an extremely slow precession has large cumulative effect on the direction of the quadrupole at second order), the effect of misalignement is excuisitively sensitive to magnetic fields in the IGM at redshifts prior to cosmic reionization—as we show in Paper I, a miniscule magnetic field strength of 10^{-21} Gauss (in comoving units) produces order-one changes in the direction of the quadrupole. This means that a high-precision measurement of the 21-cm brightness-temperature 2-point correlation function intrinsically has that level of sensitivity to detecting magnetic fields in the Dark Ages. We now proceed to develop a formalism to search for this effect, with future surveys of redshifted 21-cm line, and to identifying experimental setups that can reach it.

III. BASICS

Before focusing on the estimator formalism in the next Section, here we review the basics of cosmological estimation with 21-cm temperature fluctuation measurements. In §III A, we review definitions of quantities describing sensitivity of interferometric radio arrays; in §III B, we particularly focus on teh derivation of the noise power spectrum; and in §III C, we discuss the effects of teh array configuration and its relation to coverage of modes in the uv plane of the array.

A. Definitions

The redshifted 21-cm signal can be represented as a specific intensity at the location in physical space $I(\vec{r})$, or in Fourier space $\widetilde{I}(\vec{k})$. In sky coordinates (centered on an emitting patch of the sky), these functions become $\mathcal{I}(\theta_x, \theta_y, \theta_\nu)$, and $\widetilde{\mathcal{I}}(u, v, \eta)$, respectively. Here, vector $\vec{k}$ (in the units of comoving Mpc^{-1}) is a Fourier dual of $\vec{r}$ (comoving Mpc), and likewise, θ_x (rad), θ_y (rad), and θ_ν (Hz) are duals of the coordinates in the uv-plane u (rad^{-1}), v (rad^{-1}), and η (seconds), respectively. Notice that θ_x and θ_y represent the angular extent of the patch in the sky, while θ_ν represents its extent in the frequency space. The two sets of coordinates are related through linear transformations in the following way

$$
\begin{aligned}
\theta_x &= \frac{r_x}{D_M(z)}, & u &= \frac{k_x D_M(z)}{2\pi}, \\
\theta_y &= \frac{r_y}{D_M(z)}, & v &= \frac{k_y D_M(z)}{2\pi}, \\
\theta_\nu &= \frac{H(z)\nu_{21}}{c(1+z)^2} r_z, & \eta &= \frac{c(1+z)^2}{2\pi H(z)\nu_{21}} k_z,
\end{aligned}
\tag{2}
$$

where ν_{21} is the 21-cm frequency in the rest frame, $H(z)$ iz the Hubble parameter, $D_M(z)$ is the comoving distance in transverse direction, and z is the reference redshift in the middle of the observed data cube (where r_z and θ_ν intervals are evaluated). Note that conditions of the type $2\pi\theta_x u = r_x k_x$ are saticefied.

The convention we use for the Fourier transforms is (note that Fourier-space functions are denoted with tilde)

$$
\begin{aligned}
I(\vec{r}) &= \int \widetilde{I}(\vec{k}) e^{i\vec{k}\cdot\vec{r}} d^3\vec{k}, \\
\widetilde{I}(\vec{k}) &= \frac{1}{(2\pi)^3} \int I(\vec{r}) e^{-i\vec{k}\cdot\vec{r}} d^3\vec{r},
\end{aligned}
\tag{3}
$$

and similarly,

$$
\begin{aligned}
\mathcal{I}(\theta_x, \theta_y, \theta_\nu) &= \int \widetilde{\mathcal{I}}(u, v, \eta) e^{2\pi i(u\theta_x + v\theta_y + \eta\theta_\nu)} du dv d\eta, \\
\widetilde{\mathcal{I}}(u, v, \eta) &= \int \mathcal{I}(\theta_x, \theta_y, \theta_\nu) e^{-2\pi i(u\theta_x + v\theta_y + \eta\theta_\nu)} d\theta_x d\theta_y d\theta_\nu .
\end{aligned}
\tag{4}
$$

The following scaling relation is saticefied

$$
\widetilde{I}(\vec{k}) = \frac{c(1+z)^2 D_M(z)^2}{(2\pi)^3 H(z)\nu_{21}} \widetilde{\mathcal{I}}(u, v, \eta),
\tag{5}
$$

where the proportionallity factor is a Jacobian $\frac{d\theta_x d\theta_y d\theta_\nu}{dr_x dr_y dr_z}$.

Finally, the relationship between the specific intensity in the uv-plane and the visibility function $V(u, v, \theta_\nu)$ is given by a Fourier transform over only the frequency coordinate,

$$
\begin{aligned}
V(u, v, \theta_\nu) &= \int \widetilde{\mathcal{I}}(u, v, \eta) e^{2\pi i\theta_\nu \eta} d\eta, \\
\widetilde{\mathcal{I}}(u, v, \eta) &= \int V(u, v, \theta_\nu) e^{-2\pi i\theta_\nu \eta} d\theta_\nu,
\end{aligned}
\tag{6}
$$

Here, θ_ν is a discrete variable such that $\theta_{\nu,\max} - \theta_{\nu,\min} = \Delta\nu$ is the bandwidth of the observed data cube centered on z (see also Appendix A).

B. Power spectra and noise

In this Section, we derive the noise power spectrum for the brightness temperature signal. We start by defining a brightness-temperature power spectrum as

$$
\langle \widetilde{I}(\vec{k}) \widetilde{I}^*(\vec{k}') \rangle \equiv (2\pi)^3 P_{\widetilde{I}} \delta_D(\vec{k} - \vec{k}'),
\tag{7}
$$

where δ_D is the Dirac delta function. The observable we wish to relate this power spectrum to is the visibility function—a complex Gaussian variable with a zero mean, whose noise-induced variance (derived in Appendix A) reads

$$
\begin{aligned}
&\langle V(u, v, \theta_\nu) V(u', v', \theta'_\nu)^* \rangle \\
&= \left(\frac{2k_B T_{\rm sky}}{A_e \sqrt{\Delta\nu t_1}} \right)^2 \delta_D(u - u') \delta_D(v - v') \delta_{\theta_\nu \theta'_\nu},
\end{aligned}
\tag{8}
$$

where $T_{\rm sky}$ is the sky temperature; t_1 is the total time a single baseline spent observing an element at the position

(u, v) in the uv plane; A_e is the collecting area of a single dish; k_B is Boltzmann constant; $\Delta\nu$ is the bandwidth centered on z; and δ symbol with subscripts denotes the Kronecker delta.

The next step is to combine Eqs. (6) and (8), and take ensamble average to get

$$\begin{aligned}&\langle\widetilde{\mathcal{I}}(u,v,\eta)\widetilde{\mathcal{I}}^*(u',v',\eta')\rangle\\ &=\frac{1}{t_1}\left(\frac{2k_BT_{\rm sys}}{A_e}\right)^2\delta_D(u-u')\delta_D(v-v')\delta(\eta-\eta'),\end{aligned}\tag{9}$$

where

$$\int e^{2\pi i\theta_\nu(\eta-\eta')}d\theta_\nu=\delta_D(\eta-\eta'),\tag{10}$$

is the periodic delta-function on the t_1 interval. Taking into account the scaling relation of Eq. (5), introducing the power spectrum of Eq. (7), and keeping in mind the scaling property of the delta function, we arrive at

$$P_1^N(\vec{k})=\frac{1}{t_1}\frac{c(1+z)^2D_M^2(z)}{H(z)\nu_{21}}\left(\frac{2k_BT_{\rm sky}}{A_e}\right)^2,\tag{11}$$

for the noise per $\vec{k}$ mode, per baseline.

Computation of t_1 from the total duration of the survey $t_{\rm obs}$ depends on the type of the experiment. For a beam of a solid angle $\Omega_{\rm beam}=\lambda^2/A_e$ much smaller than the solid angle of the entire survey, $\Omega_{\rm survey}$, where telescopes scan the sky one beamwidth at a time (such as the case for radio dishes), t_1 is the total time spent observing one uv element of size corresponding to the beam size, $t_1 = t_{\rm obs}\Omega_{\rm survey}/\Omega_{\rm beam}$. However, in the case of an array of dipoles, the beam is greater or equal to the survey angular size, and $t_1 = t_{\rm obs}$. When deriving numerical results in §VI, we will assume the latter. Finally, we will not account for the fact that a given patch of the sky is only visible for a part of a day from a given location; therefore, $t_{\rm obs}$ we use in §VI is the survey duration times a factor of a few or less that corrects for this assumption.

The last step is to get from Eq. (11) to the expression for the noise power spectrum that corresponds to the observation with all the available baselines. To do that, we need to incorporate the knowledge about the array configuration and the coverage of the uv plane. In other words, we need to divide the expression in Eq. (11) by the number of baselines that see a given mode $\vec{k}$ at any given time $n_{\rm base}(\vec{k})$ (for a discussion of the uv coverage, see the following section). The final result for the noise power spectrum per mode $\vec{k}$ in the intensity units is then

$$P^N(\vec{k})=\frac{1}{t_1}\frac{c(1+z)^2D_M^2(z)}{H(z)\nu_{21}}\frac{(2k_BT_{\rm sys})^2}{A_e^2n_{\rm base}(\vec{k})},\tag{12}$$

and in temperature units

$$P^N(\vec{k})=\frac{\lambda^4}{t_1}\frac{c(1+z)^2D_M^2(z)}{H(z)\nu_{21}}\frac{T_{\rm sys}^2}{A_e^2n_{\rm base}(\vec{k})}.\tag{13}$$

C. The UV coverage

Total number density $n_{\rm base}(\vec{k})$ of baselines that can observe mode $\vec{k}$ is related to the (unitless) number density $n(u, v)$ of baselines per $dudv$ element as

$$n_{\rm base}(\vec{k})=\frac{n(u,v)}{\Omega_{\rm beam}},\tag{14}$$

where $\frac{1}{\Omega_{\rm beam}}$ represents an element in the uv plane. The number density integrates to the total number of baselines $N_{\rm base}$,

$$N_{\rm base}=\frac{1}{2}N_{\rm ant}(N_{\rm ant}+1)=\int_{\rm half}n(u,v)dudv,\tag{15}$$

where $N_{\rm ant}$ is the number of antennas in the array, and the integration is done on the half of the uv plane (because the visibility has the following property $V(u,v,\theta_\nu) = V^*(-u,-v,\theta_\nu)$, and only half the plane contains independent samples). We assume that the array consists of many antennas, so that time-dependence of $n(u, v)$ is negligible; if this is not the case, one should compute its time average to account for Earth's rotation.

Let us now consider $n_{\rm base}(\vec{k})$ for a specific array configuration that is of particualr interest to cosmology—a tightly packed array of simple dipole antennas, tiling a squared-surface of the area $(\Delta L)^2$ with a filling fraction close to one. This is a design such as the Fast Fourier Transform Telescope (FFTT) described in [32]. In this case, the beam solid angle is 1 sr, the affective area of a single dipole is $A_e = \lambda^2$, and the effective number of antennas is then $N_{\rm ant}=\frac{(\Delta L)^2}{\lambda^2}$. For such configuration

$$n(u,v)=(\frac{\Delta L}{\lambda}-u)(\frac{\Delta L}{\lambda}-v).\tag{16}$$

The relation between $\vec{k}=(k,\theta_k,\phi_k)$ and (u, v) is

$$\begin{aligned}u_\perp&\equiv\frac{D_A(z)}{2\pi}k\sin\theta_k,\\ u&=u_\perp\cos\phi_k,\\ v&=u_\perp\sin\phi_k,\end{aligned}\tag{17}$$

where subscript $\perp$ denotes components perpendicular to the LOS direction $\hat{\mathbf{n}}$, and D_A is the angular diameter distance. From this, the corresponsing number of baselines observing a given $\vec{k}$ is

$$\begin{aligned}n_{\rm base}(\vec{k})=&(\frac{\Delta L}{\lambda}-\frac{D_A(z)}{2\pi}k\sin\theta_k\cos\phi_k)\\ &\times(\frac{\Delta L}{\lambda}-\frac{D_A(z)}{2\pi}k\sin\theta_k\sin\phi_k).\end{aligned}\tag{18}$$

In §VI, we use a ϕ_k-averaged version of this quantity (between 0 and $\pi/2$ only, due to the four-fold symmetry of the experimental setup of a square of dipoles), to account for the rotation of the baselines with respect to the modes,

$$\langle n_{\rm base}(\vec{k})\rangle_{\phi_k} = \left(\frac{\Delta L}{\lambda}\right)^2 - \frac{4}{\pi}\frac{\Delta L}{\lambda}\frac{D_A(z)}{2\pi}k\sin\theta_k + \left(\frac{D_A(z)}{2\pi}k\sin\theta_k\right)^2. \tag{19}$$

IV. QUADRATIC ESTIMATOR FORMALISM

We now derive an unbiased minimum-variance quadratic estimator for a cosmic magnetic field $\vec{B}$, following a formalism similar to what is used in CMB studies [33]. We first assume that the field is uniform across the survey volume, and only evolves with redshift due to the expansion of the universe as

$$B(z) = B_0(1+z)^2, \tag{20}$$

where B_0 represents its present-day value (or equivalently, its value in comoving units); the relevant estimator is denoted y a hat sign, $\widehat{B}_0$. Then we move on to the case of a stochastic magnetic field, with a given power spectrum $P_B(\vec{K})$ where $\vec{K}$ denotes the wavevector for the mode of the field; in this case, the relevant estimator is of its amplitude, $\widehat{A}_0$. In both cases, the presented formalism is only valid if there the following separation is scales is saticefied: density-field modes in consideration must have much smaller wavelengths than the coherence scale of the magnetic field (or a given mode of a stochastic magnetic field), and both must be smaller than the size of the tomography survey at hand.

A. Uniform field

We first derive an unbiased minimum-variance quadratic estimator $\widehat{B}_0$ for a uniform magnetic field. We start by noting that the redshifted 21-cm brightness temperature Fourier modes $T(\vec{k})$ contain contribution from the noise $T^N(\vec{k})$ and the signal $T^S(\vec{k})$, where the signal is generated both by the 21-cm signal with no magnetic field (null-case signal $T_0^S(\vec{k})$), and by the magnetic field,

$$\begin{aligned} T(\vec{k}) &= T^N(\vec{k}) + T^S(\vec{k}), \\ T^S(\vec{k}) &= T_0^S(\vec{k}) + B\frac{\partial T_0^S}{\partial B}(\vec{k}), \end{aligned} \tag{21}$$

where the magnitude of the field B is a small expansion parameter in the linear theory we adop throught this work. We use the subscript "0" to denote functions evaluated at $B = 0$. The only Gaussian random field the signal temperature is proportional to is the density fluctuation δ, with the proportionality being the transfer funtion $G\widehat{\mathbf{k}}$,

$$\begin{aligned} T^S(\vec{k}) &= G(\widehat{\mathbf{k}})\delta(k), \\ T_0^S(\vec{k}) &= G_0(\widehat{\mathbf{k}})\delta(k), \end{aligned} \tag{22}$$

where $\widehat{\mathbf{k}} = (\theta_k, \phi_k)$ is a unit vector in the direction of $\vec{k}$; while G is only a function of the direction vector $\widehat{\mathbf{k}}$, the power spectrum P_δ is only a function of the magnitude k in an isotropic universe. Note especially that we use the following notation

$$\begin{aligned} \frac{\partial T_0^S}{\partial B}(\vec{k}) &\equiv \delta(k)\frac{\partial G}{\partial B}(\widehat{\mathbf{k}}, B=0), \\ \frac{\partial G_0}{\partial B}(\widehat{\mathbf{k}}) &\equiv \frac{\partial G}{\partial B}.(\widehat{\mathbf{k}}, B=0) \end{aligned} \tag{23}$$

Furthermore, we use notation for the power spectrum in the null case,

$$P_{\rm null}(\vec{k}) \equiv P^N(\vec{k}) + P_0^S(\vec{k}), \tag{24}$$

where the signal power spectrum in the absence of magnetic fields is

$$\begin{aligned} \left\langle T_0(\vec{k})T_0^*(\vec{k}')\right\rangle &\equiv (2\pi)^3\delta_D(\vec{k}-\vec{k}')P_0^S(\vec{k}) \\ &= (2\pi)^3\delta_D(\vec{k}-\vec{k}')G_0^2(\widehat{\mathbf{k}})P_\delta(k), \end{aligned} \tag{25}$$

and

$$\left\langle \delta(\vec{k})\delta^*(\vec{k}')\right\rangle \equiv (2\pi)^3\delta_D(\vec{k}-\vec{k}')P_\delta(k). \tag{26}$$

The observable 2-point correlation function in Fourier space than becomes

$$\begin{aligned} \langle T(\vec{k})T^*(\vec{k}')\rangle &= P_{\rm null}(\vec{k})(2\pi)^3\delta_D(\vec{k}-\vec{k}') \\ &+ \langle T_0^S(\vec{k})B\frac{\partial T^{S,*}}{\partial B}(\vec{k}')\rangle + \langle T_0^{S,*}(\vec{k}')B\frac{\partial T^S}{\partial B}(\vec{k})\rangle, \end{aligned} \tag{27}$$

where we assume that the signal and the noise are uncorrelated, and keep only terms linear in B. Expanding the rhs gives

$$\begin{aligned} \langle T(\vec{k})T^*(\vec{k}')\rangle &= P_{\rm null}(\vec{k})(2\pi)^3\delta_D(\vec{k}-\vec{k}') \\ &+ 2BP_\delta(\vec{k})Re\left[G_0^*(\widehat{\mathbf{k}})\frac{\partial G_0}{\partial B}(\widehat{\mathbf{k}})\right](2\pi)^3\delta_D(\vec{k}-\vec{k}'). \end{aligned} \tag{28}$$

Notice here that, unlike the case of a uniform magnetic field, a stochastic field introduces cross correlations between otherwise independent Fourier modes in the brightness temperature signal. This produces the characteristic statistical-anisotropy signal that is a telltale signatrure of the magnetic fields in situ at high redshift.

The next step is to note that we observe only one universe, so the measured proxy for the ensamble average of Eq. (28) is just the product $T(\vec{k})T^*(\vec{k})$. Using this fact and inverting Eq. (28) gives an estimator for B from a single $\vec{k}$-mode measurement,

$$\widehat{B}_{\vec{k}} = \frac{\frac{1}{V}T(\vec{k})T^*(\vec{k}) - P_{\rm null}(\vec{k})}{2P_\delta(\vec{k})Re\left[G_0^*(\widehat{\mathbf{k}})\frac{\partial G_0}{\partial B}(\widehat{\mathbf{k}})\right]}. \tag{29}$$

Note that we used the following property of the Dirac delta function on a bound volume (volume of the survey V)

$$\delta_D(\vec{k}-\vec{k}') = \frac{V}{(2\pi)^3}, \qquad \text{for } \vec{k}=\vec{k}', \tag{30}$$

and its relation to the Kroneker delta

$$\delta_{\vec{k}\vec{k}'} = \frac{(2\pi)^3}{V}\delta_D(\vec{k}-\vec{k}'). \tag{31}$$

The estimator of Eq. (29) is unbiased, $\langle \widehat{B}_{\vec{k}} \rangle = 0$, and the above expression can be used to calculate its covariance,

$$C_{\vec{k},\vec{k}'} \equiv \langle \widehat{B}_{\vec{k}} \widehat{B}^*_{\vec{k}'} \rangle = \frac{\left\langle \left(\frac{1}{V}T(\vec{k})T^*(\vec{k}) - P_{\rm null}(\vec{k})\right)\left(\frac{1}{V}T^*(\vec{k}')T(\vec{k}') - P_{\rm null}(\vec{k}')\right)\right\rangle}{4P_\delta(\vec{k})P_\delta(\vec{k}')Re\left[G_0^*(\widehat{\mathbf{k}})\frac{\partial G_0}{\partial B}(\widehat{\mathbf{k}})\right]Re\left[G_0(\widehat{\mathbf{k}}')\frac{\partial G_0^*}{\partial B}(\widehat{\mathbf{k}}')\right]}, \tag{32}$$

The expectation value in the above equation involves temperature 4-point correlation. If we enumerate factors of "T" in this correlation as $\langle 1\ 2\ 3\ 4\rangle$, the expansion of this correlation of four Gaussian random variables can be represented as a sum of the following contractions: $\langle T(\vec{k})T^*(\vec{k})T^*(\vec{k}')T(\vec{k}')\rangle = \langle 1\ 2\rangle\langle 3\ 4\rangle + \langle 1\ 4\rangle\langle 2\ 3\rangle + \langle 1\ 3\rangle\langle 2\ 4\rangle$. Keeping this order of summands, the correlation becomes

$$\begin{aligned}&\langle T(\vec{k})T^*(\vec{k})T^*(\vec{k}')T(\vec{k}')\rangle \\ &= V^2 P_{\rm null}(\vec{k})^2\left(1+\delta_{\vec{k},\vec{k}'}+\delta_{\vec{k},-\vec{k}'}\right)\end{aligned} \tag{33}$$

where we used Eqs. (30) and (31). The rest of the terms in Eq. (32) are of the form

$$\frac{1}{V}\langle T(\vec{k})T^*(\vec{k})\rangle P_{\rm null}(\vec{k}') = P_{\rm null}(\vec{k})P_{\rm null}(\vec{k}'). \tag{34}$$

Finally, substituting Eqs. (33), (34), and (31), into Eq. (32), we get the following expression for the covariance

$$\langle \widehat{B}_{\vec{k}} \widehat{B}^*_{\vec{k}'} \rangle = \frac{P^2_{\rm null}(\vec{k})\left(\delta_{\vec{k},\vec{k}'}+\delta_{\vec{k},-\vec{k}'}\right)}{\left(2P_\delta(\vec{k})Re\left[G_0^*(\widehat{\mathbf{k}})\frac{\partial G_0}{\partial B}(\widehat{\mathbf{k}})\right]\right)^2}, \tag{35}$$

This covariance matrix is singular, and the only non-vanishing entries are those relating the same mode with itself (or to the same mode in the opposite direction), which is a consequence of the reality of the temperature field, and the isotropy of space in the null-assumption case. The usual expression for a minimum-variance estimator,

$$\widehat{B} = \frac{\sum_{\vec{k},\vec{k}'} C^{-1}_{\vec{k},\vec{k}'}\widehat{B}_{\vec{k}}}{\sum_{\vec{k},\vec{k}'} C^{-1}_{\vec{k},\vec{k}'}}, \tag{36}$$

in this case reduces to

$$\widehat{B} = \frac{1}{2}\frac{\sum_{\vec{k}} \frac{\widehat{B}_{\vec{k}}}{\sigma^2_{\vec{k}}}}{\sum_{\vec{k}} \frac{1}{\sigma^2_{\vec{k}}}}, \tag{37}$$

where, the variance is defined as $\sigma^2_{\vec{k}} \equiv \langle \widehat{B}_{\vec{k}} \widehat{B}^*_{\vec{k}} \rangle$. The factor of $\frac{1}{2}$ comes from the two Kronecker deltas in Eq. (35).

The final expression for the estimator is then

$$\widehat{B} = \frac{\sum_{\vec{k}} \frac{\frac{1}{V}T(\vec{k})T^*(\vec{k}) - P_{\rm null}(\vec{k})}{P^2_{\rm null}(\vec{k})} P_\delta(\vec{k}) Re\left[G_0^*(\widehat{\mathbf{k}})\frac{\partial G_0}{\partial B}(\widehat{\mathbf{k}})\right]}{\sum_{\vec{k}}\left(\frac{2P_\delta(\vec{k})Re\left[G_0^*(\widehat{\mathbf{k}})\frac{\partial G_0}{\partial B}(\widehat{\mathbf{k}})\right]}{P_{\rm null}(\vec{k})}\right)^2}, \tag{38}$$

and its variance is

$$\sigma^2_{\widehat{B}} = \left(\sum_{\vec{k}}\left(\frac{2P_\delta(k)Re\left[G_0^*(\widehat{\mathbf{k}})\frac{\partial G_0}{\partial B}(\widehat{\mathbf{k}})\right]}{G_0^2(\widehat{\mathbf{k}})P_\delta(k) + P^N(\vec{k})}\right)^2\right)^{-1}. \tag{39}$$

B. Stochastic field

We now a minimum-variance quadratic estimator for Fourier modes of a stochastic magnetic field. Note that in this Section we do *not* assume a particular model for its power spectrum. We use B_i to denote a component of $\vec{B}$ along one of the three Cartesian-system axes, and $\vec{x}$ to denote a position vector in physical space. We start with

$$T^S(\vec{x}) = T_0^S(\vec{x}) + B_i(\vec{x})\frac{\partial T_0^S}{\partial B_i}(\vec{x}), \tag{40}$$

where the subscripts and superscripts have the same meaning as before. Note that the distinction from the uniform field case is that B (and its components) is now a function of $\vec{x}$. We then transition to Fourier space,

$$\begin{aligned}T^S(\vec{k}) &= T_0^S(\vec{k}) + \int d\vec{x}e^{-i\vec{k}\cdot\vec{x}}B_i(\vec{x})\frac{\partial T_0^S}{\partial B_i}(\vec{x}) \\ &= T_0^S(\vec{k}) + \frac{1}{(2\pi)^3}\int d\vec{k}_1 B_i(\vec{k}_1)\frac{\partial T_0^S}{\partial B_i}(\vec{k}-\vec{k}_1),\end{aligned} \tag{41}$$

where k_1 is the integration variable, and the last step used the convolution theorem.

In this case, the observable 2-point correlation function in Fourier space becomes

$$\begin{aligned}\left\langle T(\vec{k})T^*(\vec{k}')\right\rangle &= P_{\rm null}(\vec{k})(2\pi)^3\delta_D(\vec{k}-\vec{k}')\\ &+\left\langle T_0^*(\vec{k}')\frac{1}{(2\pi)^3}\int d\vec{k}_1 B_i(\vec{k}_1)\frac{\partial T_0}{\partial B_i}(\vec{k}-\vec{k}_1)\right\rangle\\ &+\left\langle T_0(\vec{k})\frac{1}{(2\pi)^3}\int d\vec{k}_1 B_i^*(\vec{k}_1)\left(\frac{\partial T_0}{\partial B_i}(\vec{k}'-\vec{k}_1)\right)^*\right\rangle,\end{aligned} \tag{42}$$

to first order in B_i. Expanding this expression further and transitioning from Dirac to Kronecked delta in order to perform the integrals within the brakets, we get

$$\begin{aligned}\left\langle T(\vec{k})T^*(\vec{k}')\right\rangle &= (2\pi)^3\delta_D(\vec{k}-\vec{k}')P_{\rm null}(\vec{k}) + B_i(\vec{k}-\vec{k}')\\ &\times\left[P_\delta(k')G_0^*(\widehat{\mathbf{k}}')\frac{\partial G_0}{\partial B_i}(\widehat{\mathbf{k}}') - P_\delta(k)G_0(\widehat{\mathbf{k}})\frac{\partial G_0^*}{\partial B_i}(\widehat{\mathbf{k}})\right],\end{aligned} \tag{43}$$

where we also used the reality of the B_i field, $B_i^*(-\vec{K}) = -B_i(\vec{K})$. Now, if we wish to estimate $B_i(\vec{K}\equiv\vec{k}-\vec{k}')$ from $\vec{k},\vec{k}'$ pair of modes, following an analogous procedure to that used in §IV A, we get

$$\widehat{B}_i^{\vec{k}\vec{k}'}(\vec{K}) = \frac{T(\vec{k})T^*(\vec{k}')}{P_\delta(k')G_0^*(\widehat{\mathbf{k}}')\frac{\partial G_0}{\partial B_i}(\widehat{\mathbf{k}}') - P_\delta(k)G_0(\widehat{\mathbf{k}})\frac{\partial G_0^*}{\partial B_i}(\widehat{\mathbf{k}})}, \tag{44}$$

where we only focus on terms $\vec{K}\neq 0$ ($\vec{k}\neq\vec{k}'$). The variance of this estimator (evaluated under the null assumption) is

$$\left\langle \widehat{B}_i^{\vec{k}\vec{k}'}(\vec{K})\left(\widehat{B}_i^{\vec{k}\vec{k}'}(\vec{K}')\right)^*\right\rangle = \frac{\left\langle T(\vec{k})T^*(\vec{k}')T^*(\vec{k})T(\vec{k}')\right\rangle}{\left(P_\delta(k')G_0^*(\widehat{\mathbf{k}}')\frac{\partial G_0}{\partial B_i}(\widehat{\mathbf{k}}') - P_\delta(k)G_0(\widehat{\mathbf{k}})\frac{\partial G_0^*}{\partial B_i}(\widehat{\mathbf{k}}')\right)\left(P_\delta(k')G_0(\widehat{\mathbf{k}})\frac{\partial G_0^*}{\partial B_i}(\widehat{\mathbf{k}}') - P_\delta(k)G_0^*(\widehat{\mathbf{k}})\frac{\partial G_0}{\partial B_i}(\widehat{\mathbf{k}})\right)}. \tag{45}$$

Finally, using Eqs. (44) and (45), we can derive the full estimator for the mode $B_i(\vec{K})$, in the usual way (by combining the individual $\widehat{B}_i^{\vec{k}\vec{k}'}(\vec{K})$ estimates with inverse-variance weights, and normalizing appropriately); as this is a straightforward exercise, we will not present this equation here. The null-case measurement of the power spectrum of B_i is the variance of its estimator, and reads

$$(2\pi)^3\delta_D(\vec{K}-\vec{K}')P^N_{B_i}(\vec{K}) \equiv \left\langle\widehat{B}_i(\vec{K})\widehat{B}_i(\vec{K}')^*\right\rangle = \left(\sum_{\vec{k}}\frac{1}{2}\frac{\left|P_\delta(k')G_0^*(\widehat{\mathbf{k}}')\frac{\partial G_0}{\partial B_i}(\widehat{\mathbf{k}}') - P_\delta(k)G_0(\widehat{\mathbf{k}})\frac{\partial G_0^*}{\partial B_i}(\widehat{\mathbf{k}})\right|^2}{V^2\left(G_0^2(\widehat{\mathbf{k}})P_\delta(k)+P^N(\vec{k})\right)\left(G_0^2(\widehat{\mathbf{k}}')P_\delta(k')+P^N(\vec{k}')\right)}\right)^{-1}, \tag{46}$$

with the restriction $\vec{K}=\vec{k}-\vec{k}'$, and where the factor of 1/2 serves to avoid double-counting mode pairs. As before, P^N is given by Eq. (13). If we limit ourselves to the diagonal terms only, $\vec{K}=\vec{K}'$, then the lhs of the above expression becomes $VP^N_{B_i}(\vec{K})$. The resulting expression for the noise power spectrum is

$$P^N_{B_i}(\vec{K}) = \left(\frac{(2\pi)^3}{2V}\sum_{\vec{k}}\frac{\left|P_\delta(k')G_0^*(\widehat{\mathbf{k}}')\frac{\partial G_0}{\partial B_i}(\widehat{\mathbf{k}}') - P_\delta(k)G_0(\widehat{\mathbf{k}})\frac{\partial G_0^*}{\partial B_i}(\widehat{\mathbf{k}})\right|^2}{\left(G_0^2(\widehat{\mathbf{k}})P_\delta(k)+P^N(\vec{k})\right)\left(G_0^2(\widehat{\mathbf{k}}')P_\delta(k')+P^N(\vec{k}')\right)}\right)^{-1}, \tag{47}$$

Note that only the components of $\vec{B}$ in the plane of the sky have an effect of the observed brightness temperature, and so the results derived in this Section hold only for those components. The noise in these two components is not correlated, and the noise in the direction along the line of sight can be considered infinite.

Finally, note that a similar type of estimator can be written down for the directions of the uniform magnetic field, and, in principle, used to recover the direction of the magnetic field in a certain patch of the sky. However, in this work we only focus on its magnitude.

V. FISHER ANALYSIS

We now use the key results of §IV to discuss estimation of sensitivity of future observations to detecting magnetic fields in the IGM at high redshifts. We first discuss the case of a field uniform in the entire survey volume, starting with the unsatured case, where the strength of $\vec{B}$ classically produces less than 1 radian of precession at all redshifts of interest, and then move on to discussing detectability in the saturated case, where $\vec{B}$ is a strong field in this sense. Finally, we discuss detectability of a stochastic magnetic field with a scale-independent power spectrum.

A. Uniform field case

If an experiment measures the redshifted 21-cm brightness temperature, and thus provides an estimate of its 2-point statistic, its sensitivity to recovering B is given by the usual Fisher formula []. For a case of the uniform field, where Eq. (20) holds, the sensitivity σ_{B_0} to measuring B_0 is directly derived from Eq. (38),

$$
\begin{aligned}
\sigma_{B_0}^{-2}(z) &= \int dV_{\rm patch}(z)\frac{d\vec{k}}{(2\pi)^3}\left(\frac{\frac{\partial P^S}{\partial B_0}(\vec{k})}{P^N(\vec{k})+P_0^S(\vec{k})}\right)^2 \\
&= \int dV_{\rm patch}(z)\frac{k^2 dk d\phi_k \sin\theta_k d\theta_k}{2(2\pi)^3}(1+z)^2 \\
&\times\left(\frac{2P_\delta(k,z)G_0(\theta_k,\phi_k,z)\frac{\partial G_0}{\partial B}(\theta_k,\phi_k,z)}{P^N(k,\theta_k,z)+P_\delta(k,z)G_0^2(\theta_k,\phi_k,z)}\right)^2,
\end{aligned}
\tag{48}
$$

where we transitioned from a sum over $\vec{k}$ modes to an integral, using $\sum_{\vec{k}} \to V\int d\vec{k}/(2\pi)^3$. Note that we made dependence on the redshift explicit. Furthermore, the integral is performed over $V_{\rm patch}$, the comoving volume of the survey, where

$$
dV_{\rm patch} = \frac{c}{H(z)}D_A^2(z)\Omega_{\rm survey}dz, \tag{49}
$$

where D_A is angular diameter distance to z. Note again that we operate under the null assumtion of small B, so every summand in the above equation is evaluated for a fiducial case of $B=0$. In this case, the above expression can be used to compute magnitude of B detectable at 1σ level for a given noise level (and cosmology). The power spectrum of the 21-cm signal is in the denominator of the summands in order to account for sample variance. A perhaps unusual feature of this analysis is that we do not take the average of the noise over ϕ_k; this is because the magnetic field introduces anisotropy in the signal. The integration limits in Eq. (48) are: $\phi_k \in [0,2\pi]$; $\theta_k\in[0,\pi]$; and $k\in[2\pi u_{\rm min}/(d_A\sin\theta_k), 2\pi u_{\rm max}/(d_A\sin\theta_k)]$, where $u_{\rm min,max} = \frac{L_{\rm min,\ max}}{\lambda}$ correspond to the maximum and minimum baseline, respectively.

The integral in Eq. (48) is performed on a small, approximately flat, patch of the sky. If the survey area is big enough that this approximation does not hold in the entire survey patch, then this integral should be performed on small parts of the survey, and the results added in quadriture to obrain the sensitivity of the entire survey. This will then account for the change in the angle that a uniform field $\vec{B}$ makes with a line of sight, as the line of sight moves through a large survey area, and the total sensitivity is given with

$$
\begin{aligned}
\sigma_{B_0,\ \rm survey}^{-2} &= \frac{\sigma_{B_0}^{-2}}{\Omega_{\rm patch}}\int_0^{\theta_{\rm survey}}\int_0^{2\pi}\cos^2\theta d\theta d\phi \\
&= \frac{\sigma_{B_0}^{-2}\pi}{\Omega_{\rm patch}}\left(\theta_{\rm survey}+\cos\theta_{\rm survey}\sin\theta_{\rm survey}\right).
\end{aligned}
\tag{50}
$$

In the saturated case, we would be unable to measure the exact magnitude of B, but a slightly different inquiry becomes interesting. Namely, it is useful to know how sensitive are future experiments to distinguishing staturated case from zero magnetic field. To answer this question, we can write the signal power spectrum as a sum of the contributions from the case $B=0$ and from the saturated case scenario of a very strong field (denoted as infinity),

$$
P^S(\vec{k}) = (1-\xi)P^S(\vec{k},B=0)+\xi P^S(\vec{k},B\to\infty). \tag{51}
$$

We can then perform the standard Fisher analysis, completely analogous to the unsaturated case, in order to understand constraints on parameter ξ. In this case, σ_ξ would give a 1σ sensitivity to simply detecting a strong magnetic field.

B. Stochastic field case

Let us now discuss the case of a stochastic field. Using Eq. (47), with a procedure analogous to the case of a uniform field, we get

$$P^N_{B_i}(\vec{K}) = \left(\frac{1}{2}\int k^2 dk \sin\theta_k d\theta_k d\phi_k \frac{\left|P_\delta(k')G_0^*(\widehat{\mathbf{k}}')\frac{\partial G_0}{\partial B_i}(\widehat{\mathbf{k}}') - P_\delta(k)G_0(\widehat{\mathbf{k}})\frac{\partial G_0^*}{\partial B_i}(\widehat{\mathbf{k}})\right|^2}{\left(G_0^2(\widehat{\mathbf{k}})P_\delta(k) + P^N(\vec{k})\right)\left(G_0^2(\widehat{\mathbf{k}}')P_\delta(k') + P^N(\vec{k}')\right)}\right)^{-1}, \tag{52}$$

with the condition $\vec{k}' = \vec{K} - \vec{k}$.

To simplify the calculation, in the following, we only focus on signal-to-noise ratio (SNR) for detecting a particular model of magnetic field power spectrum. Namely, we consider the case where most of the signal comes from the largest modes (smallest $\vec{K}$'s). In this (squeezed) limit, $\vec{K} \ll \vec{k}$ and thus $\vec{k} \approx \vec{k}'$, such that the noise power spectrum of Eq. (52) becomes white noise (independent on $\vec{K}$). If we further denote pixels with Greek indicies, and, as before, retain Roman indicies for components of $\vec{B}$, then the pixel-noise variance for measuring a single mode $\vec{K}$ of B_i component is $\sigma^2_{B_i} \equiv P^N_{B_i}(z)/V_{\rm voxel}$, where $V_{\rm voxel}$ is volume of a survey voxel (3d pixel). The model for the power spectrum is defined through

$$(2\pi)^3\delta_D(\vec{K}-\vec{K}')P_{B_iB_j}(\vec{K}) = \left\langle B_i^*(\vec{K})B_j(\vec{K}')\right\rangle, \tag{53}$$

which relates to the variance in the transverse component $P_B(\vec{K})$ as

$$P_{B_iB_j}(\vec{K}) = (\delta_{ij} - \widehat{K}_i\widehat{K}_j)P_B(\vec{K}), \tag{54}$$

where $\widehat{K}_{i/j}$ is a unit vector along the direction of a $B_{i/j}$ component. In this discussion, as a model example, we consider a scale-independent (SI) power spectrum, were

$$P_B(\vec{K}) = A_0^2/K^3, \tag{55}$$

and the amplitude A_0 is a free parameter in units of Gauss.

To compute SNR for measuring the amplitude of an arbitrary power-spectrum model in a given redshift slice z, we have to perform a sum over all voxels in the survey volume at that z. The general expression for SNR is

$${\rm SNR}^2 = \frac{1}{2}Tr\left(N^{-1}SN^{-1}S\right), \tag{56}$$

where S is the signal matrix, N is the noise matrix. In our case, these matrices are $3N_{\rm voxels}\times 3N_{\rm voxels}$ (assuming there are $N_{\rm voxels}$ voxels in the entire survey, and that there are 3 components of $\vec{B}$). In the null case, voxels are independent, and so the noise matrix is diagonal, and the signal is the 3d power spectrum of the vector field $\vec{B}$. For a single redshift slice, this evaluates to

$$\begin{aligned}{\rm SNR}^2(z) &= \frac{1}{2}\sum_{i\alpha,j\beta}\frac{S^2_{i\alpha,j\beta}}{P^N_{B_i}(\vec{K},z)P^N_{B_j}(\vec{K},z)}V^2_{\rm voxel}\\ &= \frac{1}{2}\sum_{ij}\int d\vec{r}_\alpha\int d\vec{r}_\beta\frac{\langle B_i(\vec{r}_\alpha)B_j(\vec{r}_\beta)\rangle^2}{P^N_{B_i}(\vec{K},z)P^N_{B_j}(\vec{K},z)},\end{aligned} \tag{57}$$

where $\vec{r}_{\alpha/\beta}$ represents spatial position of a given voxel, and the expectation value on the rhs of the above equation relates to the model power spectrum. If homogeneity and isotropy are satisfied, the integrand should only depend on the separation vector $\vec{s} \equiv \vec{r}_\beta - \vec{r}_\alpha$, which gives[1]

$$\begin{aligned}{\rm SNR}^2(z) &= \frac{1}{2}\sum_{ij}\frac{dV_{\rm patch}}{(P^N_{B_i}(z))^2}\int d\vec{s}\,\langle B_i(\vec{r}_\beta-\vec{s})B_j(\vec{r}_\beta)\rangle^2\\ &= \frac{1}{2(2\pi)^3}\sum_{ij}\frac{dV_{\rm patch}}{(P^N_{B_i}(z))^2}\int d\vec{K}\left(P_{B_iB_j}(\vec{K})\right)^2(1+z)^{-8},\end{aligned} \tag{58}$$

where $dV_{\rm patch}$ is the volume of a redshift-slice patch at z, given by Eq. (49). Note that we use the power spectrum of a comoving field B, such that the redshift evolution factors out in the usual way, described in the uniform-field case. Substituting Eq. (55), and integrating over all z's available in the survey,

$$\begin{aligned}{\rm SNR}^2 = &\frac{A_0^4}{2(2\pi)^3}\int_{z_{\rm min}}^{z_{\rm max}}\frac{dV_{\rm patch}}{(P^N_{B_i}(z))^2}(1+z)^{-8}\int_0^\pi\sin\theta d\theta\\ &\int_0^{2\pi}d\phi\int_{K_{\rm min}(z,\theta,\phi)}^{K_{\rm max}(z,\theta,\phi)}\frac{dK}{K^4}\sum_{ij\in\{xx,xy,yx,yy\}}(\delta_{ij}-\widehat{K}_i\widehat{K}_j)^2,\end{aligned} \tag{59}$$

where

$$\widehat{K}_x = \sin\theta\sin\phi,\ \ \widehat{K}_y = \sin\theta\cos\phi. \tag{60}$$

The sum in the above expression reduces to

$$\sum_{ij\in\{xx,xy,yx,yy\}}(\delta_{ij}-\widehat{K}_i\widehat{K}_j)^2 = 2-\sin^2\theta(1+\sin^2\phi\cos^2\phi). \tag{61}$$

Substituting this into Eq. (59), we get

$$\begin{aligned}{\rm SNR}^2 = &\frac{A_0^4}{2(2\pi)^3}\int_{z_{\rm min}}^{z_{\rm max}}\frac{dV_{\rm patch}}{(P^N_{B_i}(z))^2}(1+z)^{-8}\int_0^\pi d\theta\\ &\int_0^{2\pi}d\phi(2-\sin^2\theta(1+\sin^2\phi\cos^2\phi))\int_{K_{\rm min}(z,\theta,\phi)}^{K_{\rm max}(z,\theta,\phi)}\frac{dK}{K^4}.\end{aligned} \tag{62}$$

Finally, performing the integration over K,θ,ϕ analitically, for the FFTT case gives

$${\rm SNR}^2 = \frac{7A_0^4}{36\pi}\int_{z_{\rm min}}^{z_{\rm max}}\frac{dV_{\rm patch}}{(P^N_{B_i}(z))^2}(1+z)^{-8}\left(\frac{1}{K^3_{\rm min}}-\frac{1}{K^3_{\rm max}}\right), \tag{63}$$

[1] Note that in the last step we used $\int d\vec{s}|f(\vec{s})|^2 = \int\frac{d\vec{K}}{(2\pi)^3}|\widetilde{f}(\vec{K})|^2$, for an arbitrary function f and its Fourier transform $\widetilde{f}$.

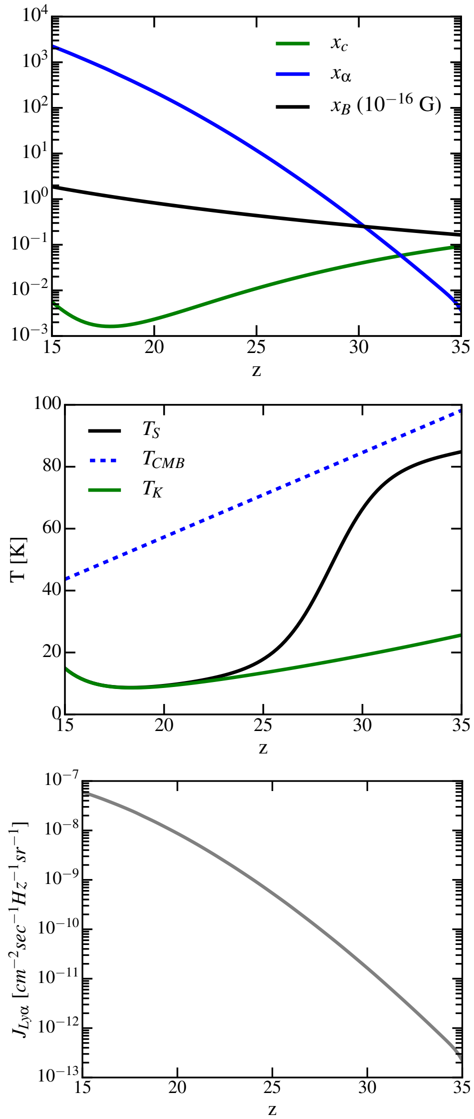

Figure 3. Inputs for sensitivity calculations: Lyman-α flux model, and the relevant spin- and kinetic- temperature models.

where $P^N_{B_i}$ is given by Eq. (52); as before, $K_{\min}$ is taken to correspond to the largest mode that fits a given survey volume, $K_{\min} = 2\pi/d_A$, and $K_{\max} = \Delta L/\lambda(z)$ (note that the numerical value of $K_{\max}$ makes very little difference in the total value of this integral). When the last expression is evaluated at $A_0 = 1$, it provides the inverse of a value of A_0 detectable at 1σ sensitivity with a given experiment.

VI. RESULTS

We now proceede to numerically evaluate the sensitivity of a tomographic 21-cm survey to detecting magnetic fields during the pre-reionization epoch, using the formalism of previous two Sections. For the purposes of

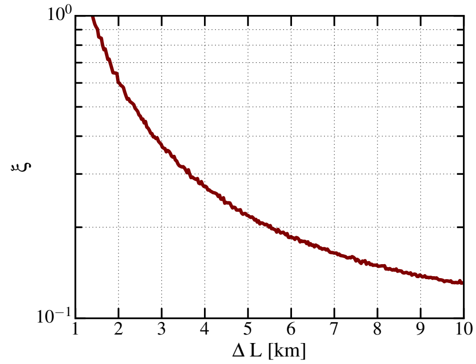

Figure 4. FFTT sensitivity to distinguishing saturated case from no magnetic field (upper panel), as a function of maximum array baseline, assuming a survey size of 1 sr, for survey duration of 2 years.

deriving numerical results, we only focus on one type of experimental setup—an array of closely-packed dipole antennas, such as the FFTT considered in §III C. The motivation for this choice is the fact that such configuration is known to maximize sensitivity of measurements based on the 2-point statistics [32], such as the one we propose in this work. For the parameters of this survey, we assume that a surface area of $(\Delta L\ \mathrm{km})^2$ is covered in dipole antennas, and that the experiment observes $\Omega_{\rm survey} = 1$sr of the sky for about 5 years.[2] For the sky temperature that enters the calculation of the noise power spectrum in Eq. (13), we assume a simple model of Galactic foregrounds from [34], where

$$T_{\rm sky} = 60 \left(\frac{21}{100} (1+z) \right)^{2.55} \ [\mathrm{K}]. \tag{64}$$

Furthermore, we assume that the redshift range covered by the survey is $z \in [15, 35]$. Other ingredients entering the sensitivity calculation are the Lyman-α flux $J_{\rm Ly\alpha}(z)$, and the spin and kinetic temperatures of the IGM; these are obtained using `21CMFAST` [35], for standard cosmology, and are shown in Figure 3. We checked that the variation in the x-ray heating rate within a factor of a few from the fiducial model does not make significant changes to the presented results.

Figures 4 and 5 show how the sensitivity changes as a function of the maximum baseline ΔL (since different baselines may correspond to different stages of the experiment). Figure 4 shows 1σ sensitivity to measuring parameter ξ of Eq. (51), that distinguishes amongst the zero magnetic field case and the case where the field is strong enough that the signal saturates (in the sense

[2] The value used to evaluate Fisher formulas is actually 2 years. When corrected for the effect of Earth's rotation, and the fact that a given sky patch is above the horizon for only a fraction of a day, the effective observation time of 2 years translates to a (factor-of-a-few) longer wall-clock time.

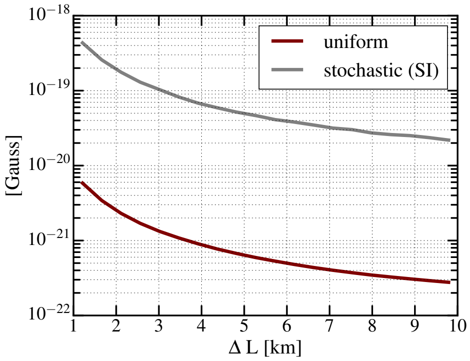

Figure 5. FFTT sensitivity to detecting a uniform and stochastic magnetic field (stochastic field is assumed to have a scale-independent (SI) power spectrum, and shown is the rms per $logK$, A_0/π.), as a function of maximum array baseline, assuming a survey size of 1 sr, for survey duration of 2 years.

described in §II). This parameter is by definition boud between the values of 0 and 1, where 0 represents the case of no magnetic field, and 1 represents the saturated case. From this Figure, we can see that, for example, a little over a square kilometer of covarega area is necessary for a 1σ detection of magnetic fields stronger than about 10^{-21} Gauss comoving. While this size of a radio array is still futuristic in terms of the shear number of antennas (compare to the SKA [27], for example), the number of mode measurements required for this measurement corresponds to the computational demands for the next-generation 21-cm cosmology experiment, and may thus be feasible in the coming couple of decades.

Figure 5 is obtained by evaluating the expressions of Eqs. (48) and (63), and shows sensitivity to measuring the scaled value of the magnetic field in the case of a uniform field (dark red line), and the sensitivity to measuring the amplitude of a particular model for a stochastic field (gray line)—the scale-independent (SI) power spectrum discussed in §V. While the numerical calculation behind this plot assumed that the brightness temperature is a linear function of the field strength, this assumption is not guaranteed to hold—it breaks in the saturation limit, as discussed in §II. In order to understand how the constraints (or, sensitivities) of Figure 5 compare to the saturation "ceiling" at the redshifts we integrate over, we present a rough calculation of the saturation as a function of redshift, and compare it to the values of the z-dependent integrands of Eq. (48). From this Figure, we can see that only above the coverage of about 16km^2 are we able to actually measure the exact value of the amplitude of the magnetic field power spectrum.

VII. CONCLUSIONS

In Paper I of this series, we proposed a new method to detect extremely weak magnetic fields in the IGM during the Dark Ages, using future 21-cm tomography experiments. In this paper, Paper II, we investigated sensitivity of future radio arrays using this method. We developed minimum-variance-estimator formalism that uses 2-point correlation function of the 21-cm brightness temperature to detect and measure magnetic fields in pre-reionization epoch.

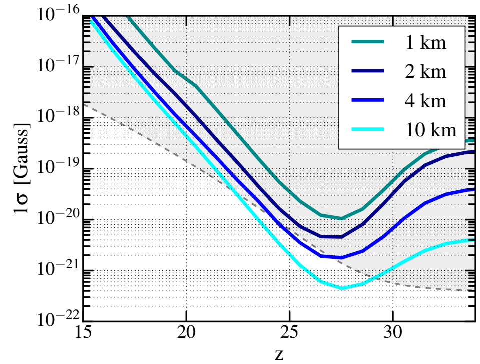

Figure 6. Saturation ceiling is shown as a shaded gray area, and integrand of Eq. (48) (inverse sqare root of it) is shown as a function of redshift, for several maximum baseline sizes. When the colored curves are below the saturation limit around their minima, the analysis assuming unsaturated regime is valid.

Our results imply that the next-stage array with a little over a square kilometer of area covered in dipole antennas ina tightly-packed configuration, observing redshifts from 15 to 35, can in principle reach the sensitivity to detect magnetic fields on the order of 10^{-21} Gauss comoving. However, disentangling teh exact spectral shape of a stochastic field is more challenging, and can only be expected in the futuristic scenarios where arrays grow to a size of tens of square kilometers in coverage area. In this analysis, we took into account the noise arising from the presence of the large Galactic foreground signal, but we ignotered more subtle effects such as, for example, frequency dependence of the beams, etc., calculation of which would be necessary to create figures of merit for future experiements.

At the end, we emphasize again that the main limitation to sensitivity of this method to measuring magnetic fields at high redshifts is a mere fact that it is based on a two-scattering process—as soon as quality of the 21-cm statistics reaches the levels necessary to probe second-order processes, the effect we focused on in this series of papers will immediately open up an "*in situ*" way to trace miniscule (and possibly primordial) magnetic fields with unprecedented precision.

ACKNOWLEDGMENTS

VG gratefully acknowledges the support from the W. M. Keck Foundation Fund. Illustrations in Figure 2 made

use of HEALPix [36] software package[3].

Appendix A: Visibility-variance derivation

Here we derive the variance of the visibility for an interferometric array of two antennas separated by a baseline $\vec{b} = (b_x, b_y)$, each with an effective collecting area A_e, observing a single element in uv plane for time duration t_1, in the total bandwidth $\Delta\nu = \nu_{\rm max} - \nu_{\rm min}$. This setup is shown in Figure 7. Note that modes with frequencies that differ by less than $1/t_1$ cannot be distinguished in observation time t_1, and modes with frequencies in each interval of size $1/t_1$ are "collapsed" into a discrete mode with $\nu_n = n/t_1$, where $n \in Z$. Thus, the number of measured (discrete) frequencies is $N_\nu = t_1\Delta\nu$.

Electric field induced in a single antenna is

$$E(t) = \sum_{n}^{N_\nu} \widetilde{E}(\nu_n) e^{2\pi i \nu_n t}, \tag{A1}$$

while the quantity an interferometer measures is the correlation coefficient between the electric field in one, E_i, and the electric field in the other antenna, E_j, as a function of frequency,

$$\rho_{ij}(\nu) \equiv \frac{\langle \widetilde{E}_i^*(\nu)\widetilde{E}_j(\nu)\rangle}{\sqrt{\langle|\widetilde{E}_i(\nu)|^2\rangle\langle|\widetilde{E}_j(\nu)|^2\rangle}}. \tag{A2}$$

Let us now assume that

$$\langle \widetilde{E}_i^*(\nu_n)\widetilde{E}_j(\nu_m)\rangle = \sigma(\nu)^2\delta_{mn}, \tag{A3}$$

In the following, for clarity, we will omit writing the explicit dependence on ν. The real (or imaginary) part of ρ has the following variance

$$\begin{aligned} &var(Re[\rho_{ij}]) \\ &= \frac{1}{(2\sigma^2)^2} var(\langle Re[\widetilde{E}_i]Re[\widetilde{E}_j] + Im[\widetilde{E}_i]Im[\widetilde{E}_j]]\rangle) \\ &= \frac{2\sigma^2\sigma^2}{(2\sigma^2)^2} = \frac{1}{2N_\nu} = \frac{1}{2t_1\Delta\nu}. \end{aligned} \tag{A4}$$

Before continuing, let us take a brief digression to show that the above formula implicitly assumes that the electric fields in the two antennas $\widetilde{E}_i$ and $\widetilde{E}_j$ have a very weak correlation, $\rho \ll 1$. Namely, suppose x and y are random Gaussian variables with zero mean values, where $var(x) \equiv \langle (x - \langle x\rangle)^2\rangle = \langle x^2\rangle - \langle x\rangle^2 = \langle x^2\rangle$, and similarly for y, and their correlation coefficient is $\rho \equiv \frac{\langle xy\rangle}{\sqrt{\langle x^2\rangle\langle y^2\rangle}}$. In this case, the following is true

$$\begin{aligned} var(xy) &= \langle x^2y^2\rangle - \langle xy\rangle^2 = \langle x^2\rangle\langle y^2\rangle + \langle xy\rangle^2 \\ &= \langle x^2\rangle\langle y^2\rangle + \rho^2\langle x^2\rangle\langle y^2\rangle = var(x)var(y)(1+\rho^2), \end{aligned} \tag{A5}$$

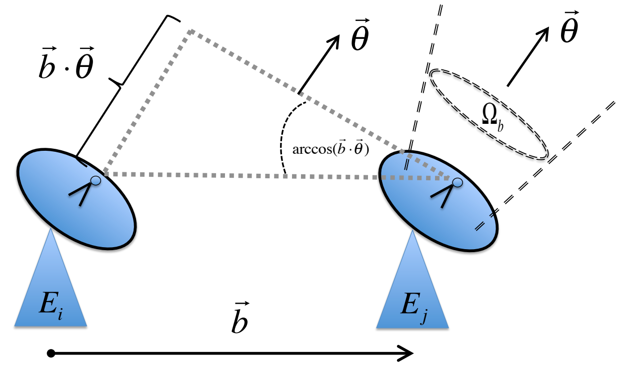

Figure 7. Two-antennae interferometer.

so that when ρ is small $var(xy) = var(x)var(y)$, which was assumed in the first equality of Eq. (A4).

Resuming the derivation, if different frequencies are uncorrelated, the result of Eq. (A4) implies

$$\langle|\rho_{ij}(\nu)|^2\rangle = \frac{1}{t_1\Delta\nu}. \tag{A6}$$

The final step in this derivation requires the relation between intensity in the sky $\mathcal{I}(\theta_x, \theta_y, \nu)$ (within the beam of the solid angle Ω_b, centered on the direction (θ_x, θ_y)) and the electric fields measured in the two antennas,

$$\begin{aligned} \langle \widetilde{E}_i^*(\nu)\widetilde{E}_j(\nu)\rangle \propto &\int_{\Omega_b} d\theta_x d\theta_y \mathcal{I}(\theta_x, \theta_y, \theta_\nu) \\ &\times e^{i\frac{2\pi\nu}{c}(b_x\theta_x + b_y\theta_y)} R(\theta_x, \theta_y), \end{aligned} \tag{A7}$$

where $R(\theta_x, \theta_y)$ is the antenna response function (the shape of the beam in the sky), which we will assume to be unity. Furthermore, $\frac{2\pi\nu}{c}(b_x\theta_x + b_y\theta_y) \equiv 2\pi(u\theta_x + v\theta_y)$ is the phase delay between two antennae (position in the uv plane measures the phase lag between the two dishes in wavelenghts). The coefficient of proportionallity in the above equation is set by various instrumental parameters, and is not relevant for our purposes. From Eq. (A2), it follows

$$\rho_{ij}(\nu) = \frac{\int_{\Omega_b} d\theta_x d\theta_y \mathcal{I}(\theta_x, \theta_y, \theta_\nu) e^{2\pi i(u\theta_x + v\theta_y)}}{\int_{\Omega_b} d\theta_x d\theta_y \mathcal{I}(\theta_x, \theta_y, \theta_\nu)}, \tag{A8}$$

where the denominator in the above formula approximately integrates to (for a small beam)

$$\int_{\Omega_b} d\theta_x d\theta_y \mathcal{I}(\theta_x, \theta_y, \theta_\nu) \approx \Omega_b \mathcal{I}(\theta_x, \theta_y, \theta_\nu). \tag{A9}$$

We can now use the approximate expression for the resolution of a single dish,

$$\Omega_b = \frac{\lambda^2}{A_e}, \tag{A10}$$

[3] http://healpix.sf.net; https://github.com/healpy/healpy

the Reyliegh-Jeans law (or the definition of the brightness temperature),

$$\mathcal{I}(\theta_x, \theta_y, \theta_\nu) = \frac{2k_B T_{\rm sky}}{\lambda^2}, \tag{A11}$$

and note that the numerator in Eq. (A8) matches the definition of visibility from Eq. (6) to get

$$\rho_{ij}(\nu) = \frac{A_e}{2k_B T_{\rm sky}} V(u, v, \theta_\nu), \tag{A12}$$

Combining the above expression and Eq. (A6), we get the final result of this derivation,

$$\langle |V(u, v, \theta_\nu)|^2 \rangle = \left(\frac{2k_B T_{\rm sky}}{A_e \sqrt{t_1 \Delta\nu}} \right)^2 \delta(u - u')\delta(v - v')\delta_{\theta_\nu \theta_{\nu'}}, \tag{A13}$$

where V is a complex Gaussian variable, centered at zero, and uncorrelated for different values of its arguments.

It should be noted at the end that we were calculating the contribution to the visibility from the noise only (the system + the foregrounds in the absence of a signal), so we used system temperature for brightness temperature (this could contain the signal from foregrounds and from the instrument). In case we want to repeat the computation in the presence of a signal, $T_{\rm sky}$ should instead be the sum of the signal and the noise temperatures.

[1] R. Durrer and A. Neronov, Astron. and Astrophys. Review **21**, 62 (2013), arXiv:1303.7121 [astro-ph.CO].

[2] J. P. Vallee, New Astronomy Reviews **48**, 763 (2004).

[3] A. Neronov and I. Vovk, Science **328**, 73 (2010), arXiv:1006.3504 [astro-ph.HE].

[4] R. Wielebinski, in *Cosmic Magnetic Fields*, Lecture Notes in Physics, Berlin Springer Verlag, Vol. 664, edited by R. Wielebinski and R. Beck (2005) p. 89.

[5] R. Beck, Space Science Reviews **166**, 215 (2012).

[6] K. Park, E. G. Blackman, and K. Subramanian, Phys. Rev. E **87**, 053110 (2013), arXiv:1305.2080 [physics.plasm-ph].

[7] S. Naoz and R. Narayan, Physical Review Letters **111**, 051303 (2013), arXiv:1304.5792 [astro-ph.CO].

[8] S. Naoz and R. Narayan, Physical Review Letters **111**, 051303 (2013), arXiv:1304.5792 [astro-ph.CO].

[9] L. M. Widrow, D. Ryu, D. R. G. Schleicher, K. Subramanian, C. G. Tsagas, and R. A. Treumann, Space Science Reviews **166**, 37 (2012), arXiv:1109.4052 [astro-ph.CO].

[10] T. Kobayashi, Journal of Cosmology and Astroparticle Physics **5**, 040 (2014), arXiv:1403.5168.

[11] D. G. Yamazaki, K. Ichiki, T. Kajino, and G. J. Mathews, Advances in Astronomy **2010** (2010), arXiv:1112.4922 [astro-ph.CO].

[12] P. Blasi, S. Burles, and A. V. Olinto, Astrophysical Journal, Letters **514**, L79 (1999), astro-ph/9812487.

[13] F. Tavecchio, G. Ghisellini, L. Foschini, G. Bonnoli, G. Ghirlanda, and P. Coppi, MNRAS **406**, L70 (2010), arXiv:1004.1329 [astro-ph.CO].

[14] K. Dolag, M. Kachelriess, S. Ostapchenko, and R. Tomàs, Astrophysical Journal, Letters **727**, L4 (2011), arXiv:1009.1782 [astro-ph.HE].

[15] K. E. Kunze and E. Komatsu, Journal of Cosmology and Astroparticle Physics **1**, 009 (2014), arXiv:1309.7994 [astro-ph.CO].

[16] T. Kahniashvili, Y. Maravin, A. Natarajan, N. Battaglia, and A. G. Tevzadze, Astrophys. J. **770**, 47 (2013), arXiv:1211.2769 [astro-ph.CO].

[17] M. Shiraishi, H. Tashiro, and K. Ichiki, Phys. Rev. D **89**, 103522 (2014), arXiv:1403.2608.

[18] H. Tashiro and N. Sugiyama, Mon. Not. R. Astron. Soc. **372**, 1060 (2006), astro-ph/0607169.

[19] D. R. G. Schleicher, R. Banerjee, and R. S. Klessen, Astrophys. J. **692**, 236 (2009), arXiv:0808.1461.

[20] Planck Collaboration, P. A. R. Ade, N. Aghanim, M. Arnaud, F. Arroja, M. Ashdown, J. Aumont, C. Baccigalupi, M. Ballardini, A. J. Banday, and et al., ArXiv e-prints (2015), arXiv:1502.01594.

[21] T. Venumadhav, A. Oklopcic, V. Gluscevic, A. Mishra, and C. M. Hirata, ArXiv e-prints (2014), arXiv:1410.2250.

[22] P. Madau, A. Meiksin, and M. J. Rees, Astrophys. J. **475**, 429 (1997), astro-ph/9608010.

[23] A. Loeb and M. Zaldarriaga, Physical Review Letters **92**, 211301 (2004), astro-ph/0312134.

[24] L. J. Greenhill and G. Bernardi, ArXiv e-prints (2012), arXiv:1201.1700 [astro-ph.CO].

[25] J. D. Bowman, M. F. Morales, J. N. Hewitt, and MWA Collaboration, in *American Astronomical Society Meeting Abstracts #218* (2011) p. 132.06.

[26] A. R. Parsons, A. Liu, J. E. Aguirre, Z. S. Ali, R. F. Bradley, C. L. Carilli, D. R. DeBoer, M. R. Dexter, N. E. Gugliucci, D. C. Jacobs, P. Klima, D. H. E. MacMahon, J. R. Manley, D. F. Moore, J. C. Pober, I. I. Stefan, and W. P. Walbrugh, Astrophys. J. **788**, 106 (2014), arXiv:1304.4991.

[27] C. L. Carilli, ArXiv e-prints (2008), arXiv:0802.1727.

[28] K. Vanderlinde and Chime Collaboration, in *Exascale Radio Astronomy* (2014) p. 10102.

[29] D. R. DeBoer and HERA, in *American Astronomical Society Meeting Abstracts*, American Astronomical Society Meeting Abstracts, Vol. 225 (2015) p. 328.03.

[30] H. Yan and A. Lazarian, Astrophys. J. **677**, 1401 (2008), arXiv:0711.0926.

[31] H. Yan and A. Lazarian, J. Quant. Spec. Rad. Trans. **113**, 1409 (2012), arXiv:1203.5571 [astro-ph.GA].

[32] M. Tegmark and M. Zaldarriaga, Phys. Rev. D **79**, 083530 (2009), arXiv:0805.4414.

[33] T. Okamoto and W. Hu, Phys. Rev. D **67**, 083002 (2003), astro-ph/0301031.

[34] Y. Mao, M. Tegmark, M. McQuinn, M. Zaldarriaga, and O. Zahn, Phys. Rev. D **78**, 023529 (2008), arXiv:0802.1710.

[35] A. Mesinger, S. Furlanetto, and R. Cen, Mon. Not. R. Astron. Soc. **411**, 955 (2011), arXiv:1003.3878.

[36] K. M. Górski, E. Hivon, A. J. Banday, B. D. Wandelt, F. K. Hansen, M. Reinecke, and M. Bartelmann, Astrophys. J. **622**, 759 (2005), astro-ph/0409513.